

Article

Ventricular and Atrial Pressure—Volume Loops: Analysis of the Effects Induced by Right Centrifugal Pump Assistance

Beatrice De Lazzari ¹, Attilio Iacovoni ², Massimo Capoccia ^{3,4,*} , Silvia Papa ⁵, Roberto Badagliacca ⁵, Domenico Filomena ⁵  and Claudio De Lazzari ^{6,7} 

¹ Department of Human Movement and Sport Sciences, “Foro Italico” 4th University of Rome, 00135 Rome, Italy; b.delazzari@studenti.uniroma4.it

² Department of Cardiology, ASST-Papa Giovanni XIII Hospital, 24127 Bergamo, Italy; aiacovoni@asst-pg23.it

³ Department of Cardiac Surgery, Leeds General Infirmary, Leeds Teaching Hospitals NHS Trust, Leeds LS1 3EX, UK

⁴ Department of Biomedical Engineering, University of Strathclyde, Glasgow G4 0NW, UK

⁵ Department of Clinical, Internal Anesthesiology and Cardiovascular Sciences, “Sapienza” University of Rome, 00185 Rome, Italy; silvia.papa@uniroma1.it (S.P.); roberto.badagliacca@uniroma1.it (R.B.); domenico.filomena@uniroma1.it (D.F.)

⁶ National Research Council, Institute of Clinical Physiology (IFC-CNR), 00185 Rome, Italy; claudio.delazzari@ifc.cnr.it

⁷ Faculty of Medicine, Teaching University Geometri, Tbilisi 0114, Georgia

* Correspondence: capoccia@doctors.org.uk



Citation: De Lazzari, B.; Iacovoni, A.; Capoccia, M.; Papa, S.; Badagliacca, R.; Filomena, D.; De Lazzari, C. Ventricular and Atrial Pressure—Volume Loops: Analysis of the Effects Induced by Right Centrifugal Pump Assistance.

Bioengineering **2022**, *9*, 181. <https://doi.org/10.3390/bioengineering9050181>

Academic Editors: Sharan Ramaswamy and Jun Liao

Received: 20 March 2022

Accepted: 17 April 2022

Published: 20 April 2022

Publisher’s Note: MDPI stays neutral with regard to jurisdictional claims in published maps and institutional affiliations.



Copyright: © 2022 by the authors. Licensee MDPI, Basel, Switzerland. This article is an open access article distributed under the terms and conditions of the Creative Commons Attribution (CC BY) license (<https://creativecommons.org/licenses/by/4.0/>).

Abstract: The main indications for right ventricular assist device (RVAD) support are right heart failure after implantation of a left ventricular assist device (LVAD) or early graft failure following heart transplantation. We sought to study the effects induced by different RVAD connections when right ventricular elastance (E_{ESRIGHT}) was modified using numerical simulations based on atrial and ventricular pressure–volume analysis. We considered the effects induced by continuous-flow RVAD support on left/right ventricular/atrial loops when E_{ESRIGHT} changed from 0.3 to 0.8 mmHg/mL during in-series or parallel pump connection. Pump rotational speed was also addressed. Parallel RVAD support at 4000 rpm with $E_{\text{ESRIGHT}} = 0.3$ mmHg/mL generated percentage changes up to 60% for left ventricular pressure–volume area and external work; up to 20% for left ventricular ESV and up to 25% for left ventricular EDV; up to 50% change in left atrial pressure–volume area ($PVLA_{L-A}$) and only a 3% change in right atrial pressure–volume area ($PVLA_{R-A}$). Percentage variation was lower when $E_{\text{ESRIGHT}} = 0.8$ mmHg/mL. Early recognition of right ventricular failure followed by aggressive treatment is desirable, so as to achieve a more favourable outcome. RVAD support remains an option for advanced right ventricular failure, although the onset of major adverse events may preclude its use.

Keywords: heart failure; RVAD; pressure-volume loop; lumped parameter model; software simulation; cardiovascular modelling; rotational pump speed; right-left heart interaction

1. Introduction

Acute right ventricular (RV) failure may develop in the context of acute decompensated heart failure, acute myocardial infarction, pulmonary embolism, fulminant myocarditis, decompensated pulmonary hypertension, post-cardiotomy shock, orthotopic heart transplant, and often after the insertion of a left ventricular assist device (LVAD) [1]. This may also be the case when a long-term right ventricular assist device (RVAD) is required for end-stage RV failure from combined pre- and post-capillary pulmonary hypertension (PH) [2].

The main indications for RVAD support are right heart failure after LVAD implantation or early graft failure following orthotopic heart transplantation. About 30–40% of patients will need RVAD support after LVAD implantation [3–6]. Markers of illness severity including evidence of end-organ dysfunction and haemodynamic profile are associated with the

need for RVAD support within two weeks following LVAD insertion [7]. The prognostic role of the right ventricle is now being acknowledged in the context of left-sided heart failure [8]. Failure of systolic function adaptation (homeometric adaptation described by Anrep's law) leads to increased dimensions (heterometric adaptation described by Starling's law) with a negative effect on diastolic ventricular interactions [9]. RV-PA coupling has significant reserve in the context of elevated RV afterload, although the level of uncoupling that leads to RV failure remains not completely defined [10]. Better understanding of the pathophysiology of right ventricular (RV) failure may well help with its initial medical management and timing of mechanical circulatory support. Prolonged survival by effective medical treatment becomes the grounds for the development of right heart failure secondary to chronic left ventricular dysfunction. Patients remain compensated as long as the right ventricle is functional. The ability to track the RV based on better monitoring of afterload and functional reserve may help change the course of the disease before the RV reaches the threshold that may limit both medical and LVAD treatment [11].

However, the lack of data does not allow for an in-depth analysis of right ventricular and atrial behaviour during RVAD support. An attempt in this direction can be made using a numerical simulator of the cardiovascular system with a view to reproduce pathological conditions requiring right ventricular assistance.

The aim of our study was the trend analysis in terms of percentage variation of the haemodynamic and energetic variables of both ventricles and atria in different cardiovascular conditions reproduced by changing right ventricular elastance from 0.3 to 0.8 mmHg/mL during RVAD support with different rotational speeds.

The first step of this work required the implementation of two new modules within CARDIOSIM© software simulation platform, which would reproduce the characteristics of the left circulatory network and a continuous flow centrifugal pump (RVAD) to be connected either in series or parallel to the right ventricle. The new modules were based on a 0-D (lumped-parameter) numerical model including input and output cannula of the RVAD.

We simulated RVAD support following in series and parallel connection driven by different rotational speeds in a heart failure setting. Subsequently, the right ventricular elastance was increased from 0.3 to 0.8 mmHg/mL in a stepwise manner. During each setting, we focused our attention on the following hemodynamic and energetic variables:

- ✓ Right and left ventricular end-systolic volume (ESV_{R-V} and ESV_{L-V});
- ✓ Right and left ventricular end-diastolic volume (EDV_{R-V} and EDV_{L-V});
- ✓ Stroke volume (SV);
- ✓ Right and left ventricular external work (EW_{R-V} and EW_{L-V}) and pressure-volume area (PVA_{R-V} and PVA_{L-V});
- ✓ Right and left atrial end-systolic volume (ESV_{R-A} and ESV_{L-A});
- ✓ Right and left atrial end-diastolic volume (EDV_{R-A} and EDV_{L-A});
- ✓ Right and left atrial pressure-volume loop area ($PVLA_{R-A}$ and $PVLA_{L-A}$);
- ✓ Cardiac output (CO);
- ✓ Systolic, diastolic, and mean systemic aortic pressure (AoP);
- ✓ Systolic, diastolic, and mean pulmonary arterial pressure (PAP);
- ✓ Pulmonary capillary wedge pressure (PCWP);
- ✓ Right and left atrial pressure (RAP and LAP).

2. Materials and Methods

2.1. The Heart and Circulatory Numerical Network

CARDIOSIM© software (Rome, Italy) platform has been previously described [12–17]. The modules of the software simulator are: systemic and pulmonary arterial section, systemic and pulmonary venous section, and coronary circulation. Native left and right ventricles, atria, and septum reproduce the entire cardiac activity; they are implemented in a single module (Figure 1) using the time-varying elastance concept [13,14]. The ventricular, atrial, and septal activity is synchronized with the electrocardiographic (ECG) signal [14]. Using

the modified time-varying elastance theory, inter-ventricular septum (IVS) interaction and instantaneous left and right ventricular pressure can be reproduced by [14,18]:

$$\begin{cases} P_{lv}(t) = \left[\frac{e_{Vsp}(t) \cdot e_{lv}(t)}{e_{lv}(t) + e_{Vsp}(t)} \right] \cdot [V_{lv}(t) - V_{lv,0}] + \left[\frac{e_{lv}(t)}{e_{lv}(t) + e_{Vsp}(t)} \right] \cdot P_{rv}(t) + \left[\frac{e_{Vsp}(t)}{e_{lv}(t) + e_{Vsp}(t)} \right] \cdot P_{lv,0} \\ P_{rv}(t) = \left[\frac{e_{Vsp}(t) \cdot e_{rv}(t)}{e_{Vsp}(t) + e_{rv}(t)} \right] \cdot [V_{rv}(t) - V_{rv,0}] + \left[\frac{e_{rv}(t)}{e_{Vsp}(t) + e_{rv}(t)} \right] \cdot P_{lv}(t) + \left[\frac{e_{Vsp}(t)}{e_{Vsp}(t) + e_{rv}(t)} \right] \cdot P_{rv,0} \end{cases} \quad (1)$$

In the same way, the inter-atrial septum (IAS) interaction and the left and right instantaneous atrial pressure can be reproduced by:

$$\begin{cases} P_{la}(t) = \left[\frac{e_{Asp}(t) \cdot e_{la}(t)}{e_{la}(t) + e_{Asp}(t)} \right] \cdot [V_{la}(t) - V_{la,0}] + \left[\frac{e_{la}(t)}{e_{la}(t) + e_{Asp}(t)} \right] \cdot P_{ra}(t) + \left[\frac{e_{Asp}(t)}{e_{la}(t) + e_{Asp}(t)} \right] \cdot P_{la,0} \\ P_{ra}(t) = \left[\frac{e_{Asp}(t) \cdot e_{ra}(t)}{e_{Asp}(t) + e_{ra}(t)} \right] \cdot [V_{ra}(t) - V_{ra,0}] + \left[\frac{e_{ra}(t)}{e_{Asp}(t) + e_{ra}(t)} \right] \cdot P_{la}(t) + \left[\frac{e_{Asp}(t)}{e_{Asp}(t) + e_{ra}(t)} \right] \cdot P_{ra,0} \end{cases} \quad (2)$$

The symbols used in Equations (1) and (2) have been listed in Table 1. These features allow the simulation of inter-ventricular and intra-ventricular dyssynchrony [19].

Table 1. Symbols used in Equations (1) and (2).

| Symbol | Description | Unit |
|-----------------------------|---|-----------------------|
| $P_{lv}(t)$ [$P_{rv}(t)$] | Instantaneous left (right) ventricular pressure | mmHg |
| $P_{lv,0}$ [$P_{rv,0}$] | Resting left (right) ventricular pressure | mmHg |
| $V_{lv}(t)$ [$V_{rv}(t)$] | Instantaneous left (right) ventricular volume | mL |
| $V_{lv,0}$ [$V_{rv,0}$] | Resting left (right) ventricular volume | mL |
| $e_{lv}(t)$ [$e_{rv}(t)$] | Left (right) ventricular elastance | mmHg·mL ⁻¹ |
| $e_{Vsp}(t)$ | Inter-ventricular septum elastance | mmHg·mL ⁻¹ |
| $P_{la}(t)$ [$P_{ra}(t)$] | Instantaneous left (right) atrial pressure | mmHg |
| $P_{la,0}$ [$P_{ra,0}$] | Resting left (right) atrial pressure | mmHg |
| $V_{la}(t)$ [$V_{ra}(t)$] | Instantaneous left (right) atrial volume | mL |
| $V_{la,0}$ [$V_{ra,0}$] | Resting left (right) atrial volume | mL |
| $e_{la}(t)$ [$e_{ra}(t)$] | Left (right) atrial elastance | mmHg·mL ⁻¹ |
| $e_{Asp}(t)$ | Inter-atrial septum elastance | mmHg·mL ⁻¹ |

Specific modules of the coronary circulation (Figure 1) are also available on the CARDIOSIM© platform [12].

For the purposes of our study, we assembled the cardiovascular network with the new module of the systemic circulation, whilst the behaviour of the heart is modelled as described in [12,13]. The systemic venous section [12,15] and the entire pulmonary circulation [16,17,20,21] are modelled as described in the current literature. We have selected the module presented in [22] for the coronary circulation. The tricuspid, mitral, pulmonary, and aortic valves are modelled with an ideal diode: when the pressure across the valve is positive, the valve opens and allows the flow of blood; when the pressure is less than or equal to zero, the valve closes and the flow of blood is zero [12–14,23].

and inferior vena cava sections, and systemic veins compartment. RVAD is the right ventricular assist device. Table 2 lists the symbols used. (b) The behaviour of the ascending aorta is simulated with resistances R_{AA} and R_{Vaa} , inertance L_{AA} and compliance C_{AA} . Q_{RAA} is the flow through the resistance and inertance. The descending aorta is implemented with resistances R_{DA} and R_{Vda} , inertance L_{DA} and compliance C_{DA} . Q_{RDA} is the flow through the resistance (R_{DA}) and inertance (L_{DA}). The carotid arteries section is reproduced with a simple resistance (R_{CA}). The superior vena cava module consists of resistances R_{SVC_I} and R_{SVC_II} , inertance L_{SCV} , and compliance C_{SVC} . The inferior vena cava module is modelled with resistances R_{IVC} , R_{IVC_I} , and R_{IVC_II} ; inertance L_{IVC} ; and compliance C_{IVC} . The intrathoracic pressure (Pt) affects compliances C_{AA} , C_{DA} , C_{IVC} , and C_{SVC} . Table 2 lists the symbols used. (c) The peripheral arteries module is modelled with resistances R_A and R_{Va} and compliance C_A . The resistor R_{Va} accounts for viscous losses of the vessels wall. Q_{RA} is the blood flow outside the compartment; it is a part of the blood that reaches the systemic veins compartment. (d) Schematic representation of RVAD connection. When the right ventricular assist device is connected in parallel, blood is removed from the right atrium ($SW_1 = ON$ and $SW_2 = OFF$) and ejected into the pulmonary artery. When RVAD is connected in series, blood is removed from the right ventricle ($SW_1 = OFF$ and $SW_2 = ON$) and ejected into the pulmonary artery. The input (output) RVAD cannula is modelled with RLC elements. Q_{oPUMP} (Q_{iPUMP}) is the output (inlet) flow rate from the pump. Q_{oCANN} (Q_{iCANN}) is the output (inlet) flow rate from the cannula. The electrical analogue of the pulmonary circulation is described in [22] (Reprinted with permission from Ref. [22], Copyright© 1991–2019 C. De Lazzari).

2.2. New Lumped-Parameter Model of the Systemic Circulation

The new module is described in Figure 1 using resistance, inertance, and compliance (RLC) elements. The systemic network consists of the following compartments: ascending and descending aorta, carotid artery, peripheral arteries, and superior and inferior vena cava (Figure 1a).

The ascending (descending) aorta is modelled using two resistances R_{AA} and R_{Vaa} (R_{DA} and R_{Vda}), inertance L_{AA} (L_{DA}), and compliance C_{AA} (C_{DA}). A single resistance (R_{CA}) reproduces the behaviour of the carotid district (Figure 1b). The peripheral arterial circulation is reproduced with resistances R_A and R_{Va} and with compliance C_A (Figure 1c). The superior vena cava compartment consists of resistances R_{SVC_I} and R_{SVC_II} , inertance L_{SVC} , and compliance C_{SVC} . The systemic venous network is implemented using compliance C_{VS} and resistances R_{VS} and R_{Vvs} (Figure 1c). Finally, the inferior vena cava district is modelled with resistances R_{IVC} , R_{IVC_I} , and R_{IVC_II} ; inertance L_{IVC} ; and compliance C_{IVC} (Figure 1b). The resistances R_{Vaa} , R_{Vda} , R_{Va} , and R_{Vvs} account for viscous losses of the vessel wall. Pt is the mean intrathoracic pressure. All the symbols of the cardiovascular network are listed in Table 2.

Table 2. Symbols of the cardiovascular network.

| | |
|-------------------------|--|
| R_{pam} (R_{pas}) | Main (small) pulmonary arterial resistance [mmHg·cm ⁻³ ·s] |
| L_{pam} (L_{pas}) | Main (small) pulmonary arterial inertance [mmHg·cm ⁻³ ·s ²] |
| C_{pam} (C_{pas}) | Main (small) pulmonary arterial compliance [mmHg ⁻¹ ·cm ⁻³] |
| MPAP (SPAP) | Main (small) pulmonary arterial pressure [mmHg] |
| R_{par} (R_{pc}) | Pulmonary arteriole (capillary) resistance [mmHg·cm ⁻³ ·s] |
| Wedge | Pulmonary capillary wedge pressure [mmHg] |
| C_{vp} | Pulmonary venous compliance [mmHg ⁻¹ ·cm ⁻³] |
| R_{vp} | Pulmonary venous resistance [mmHg·cm ⁻³ ·s] |
| PVP | Pulmonary venous pressure [mmHg] |
| R_{ro} (R_{ri}) | Pulmonary (tricuspid) valve resistance [mmHg·cm ⁻³ ·s] |
| SVP | Systemic veins pressure [mmHg] |
| C_{VS} | Systemic veins compliance [mmHg ⁻¹ ·cm ⁻³] |

Table 2. *Cont.*

| | |
|------------------------------------|---|
| R_{VS} | Systemic veins resistance [mmHg·cm ⁻³ ·s] |
| R_{Vvs} | Resistor accounting viscous losses of the systemic veins wall [mmHg·cm ⁻³ ·s] |
| R_{SVC_I} | First Superior vena cava resistance [mmHg·cm ⁻³ ·s] |
| C_{SVC} | Superior vena cava compliance [mmHg ⁻¹ ·cm ⁻³] |
| L_{SVC} | Superior vena cava inertance [mmHg·cm ⁻³ ·s ²] |
| $R_{SVC_{II}}$ | Second superior vena cava resistance [mmHg·cm ⁻³ ·s] |
| $SVCP$ | Superior vena cava pressure [mmHg] |
| $LAP(RAP)$ | Left (right) atrial pressure [mmHg] |
| $LVP(RVP)$ | Left (right) ventricular pressure [mmHg] |
| R_{AA} | Ascending aorta resistance [mmHg·cm ⁻³ ·s] |
| R_{Vaa} | Resistor accounting viscous losses of the ascending aorta wall [mmHg·cm ⁻³ ·s] |
| L_{AA} | Ascending aorta inertance [mmHg·cm ⁻³ ·s ²] |
| C_{AA} | Ascending aorta compliance [mmHg ⁻¹ ·cm ⁻³] |
| AoP | Aortic Pressure [mmHg] |
| R_{DA} | Descending aorta resistance [mmHg·cm ⁻³ ·s] |
| R_{Vda} | Resistor accounting viscous losses of the descending aorta wall [mmHg·cm ⁻³ ·s] |
| L_{DA} | Descending aorta inertance [mmHg·cm ⁻³ ·s ²] |
| C_{DA} | Descending aorta compliance [mmHg ⁻¹ ·cm ⁻³] |
| DPA | Descending aortic pressure [mmHg] |
| R_{CA} | Carotid arteries resistance [mmHg·cm ⁻³ ·s] |
| R_A | Peripheral arteries resistance [mmHg·cm ⁻³ ·s] |
| R_{Va} | Resistor accounting viscous losses of the peripheral arteries wall [mmHg·cm ⁻³ ·s] |
| C_A | Peripheral arteries compliance [mmHg ⁻¹ ·cm ⁻³] |
| PA | Peripheral arteries pressure [mmHg] |
| $R_{IVC}, R_{IVC_I}, R_{IVC_{II}}$ | Inferior vena cava resistances [mmHg·cm ⁻³ ·s] |
| L_{IVC} | Inferior vena cava inertance [mmHg·cm ⁻³ ·s ²] |
| C_{IVC} | Inferior vena cava compliance [mmHg ⁻¹ ·cm ⁻³] |
| Pt | Mean intrathoracic pressure [mmHg] |
| $ela(era)$ | Left (right) atrial elastance [mmHg/mL] |
| $elv(erv)$ | Left (right) ventricular elastance [mmHg/mL] |
| $e_{Aspt}(e_{Vspt})$ | Inter-atrial (-ventricular) septal elastance [mmHg/mL] |
| $Q_{artery}(Q_{venous})$ | Coronary arterial (venous) flow [mL/s] |
| $R_{oCANN}(R_{iCANN})$ | RVAD output (input) cannula resistance [mmHg·cm ⁻³ ·s] |
| $L_{oCANN}(L_{iCANN})$ | RVAD output (input) cannula inertance [mmHg·cm ⁻³ ·s ²] |
| $C_{oCANN}(C_{iCANN})$ | RVAD output (input) cannula compliance [mmHg ⁻¹ ·cm ⁻³] |
| $Q_{li}(Q_{lo})$ | Left ventricular input (output) flow [mL/s] |
| $Q_{ri}(Q_{ro})$ | Right ventricular input (output) flow [mL/s] |
| $Q_{lia}(Q_{ria})$ | Left (right) atrial input flow [mL/s] |

2.3. Right Ventricular Assist Device (RVAD)

A 0-D numerical model described in [16] was used to implement a centrifugal pump that reproduced the behaviour of the right ventricular assist device. The pump can be connected in series or parallel to the right ventricle with two cannulae modelled using RLC elements (Figure 1d). When the RVAD removes blood from the right atrium (parallel connection—SW1 = ON and SW2 = OFF in Figure 1d), the flow through the inlet cannula is:

$$(RAP - \Delta P) = Q_{iCANN} \cdot R_{iCANN} + \left(\frac{d}{dt} Q_{iCANN} \right) \cdot L_{iCANN} \quad (3)$$

$$\left(\frac{d}{dt} \Delta P \right) \cdot C_{iCANN} = Q_{PUMP} - Q_{iCANN} \quad (4)$$

RAP is the right atrial pressure, Li_{CANN} , Ri_{CANN} , and Ci_{CANN} are the inertance, resistance, and compliance of the inlet cannula, respectively (Figure 1d). Qi_{CANN} (Q_{PUMP}) is the flow through the inlet cannula (generated by the centrifugal pump). ΔP is the pressure on the pump head.

When the RVAD removes blood from the right ventricle (in series connection—SW1 = OFF and SW2 = ON in Figure 1d), Equation (3) becomes:

$$(RVP - \Delta P) = Qi_{CANN} \cdot Ri_{CANN} + \left(\frac{d}{dt} Qi_{CANN}\right) \cdot Li_{CANN} \quad (5)$$

RVP is the right ventricular pressure.

When the RVAD ejects blood, the flow through the outlet cannula is:

$$(\Delta P - MPAP) = Qo_{CANN} \cdot Ro_{CANN} + \left(\frac{d}{dt} Qo_{CANN}\right) \cdot Lo_{CANN} \quad (6)$$

$$\left(\frac{d}{dt} \Delta P\right) \cdot Co_{CANN} = Qo_{PUMP} - Qo_{CANN} \quad (7)$$

$MPAP$ is the mean pulmonary artery pressure (Figure 1d), Ro_{CANN} and Co_{CANN} are the inertance, resistance, and compliance of the outlet cannula, respectively. Qo_{CANN} is the flow through the outlet cannula.

2.4. Simulation Protocol

For the purposes of our simulations, we considered the values for right and left ventricular elastance that could reproduce a realistic diseased heart. According to the available literature, normal values for right ventricular elastance fluctuate around 1 mmHg/mL [24,25] and range from 1.6 to 5 mmHg/mL for left ventricular elastance [17,26]. Therefore, we considered $Ees_{LEFT} = 0.7$ mmHg/mL for the left ventricle and $Ees_{RIGHT} = 0.3$ mmHg/mL for the right ventricle as reference values for a failing heart. Our simulation approach consisted of three steps. In the first step after setting HR = 90 bpm, the slope of left ventricular End-Systolic Pressure-Volume Relationship (ESPVR) $Ees_{LEFT} = 0.7$ mmHg/mL, and the slope of right ESPVR $Ees_{RIGHT} = 0.3$ mmHg/mL [27], the simulator generated the following values: cardiac output (CO) 4.51 L/min, aortic systolic (diastolic) pressure 82.1 (60.4) mmHg, mean right atrial pressure 23.3 mmHg, pulmonary systolic (diastolic) pressure 51.2 (31.6) mmHg, and pulmonary capillary wedge pressure 20.7 mmHg. The mean pressure (flow) value was calculated as the mean value of all blood pressure (flow) measurements during a cardiac cycle.

In the second step, the slope of right ESPVR $Ees_{RIGHT} = 0.3$ mmHg/mL was set to 0.4, 0.5, 0.6, 0.7, and 0.8 mmHg/mL [10,28] and for each value the parameters described above were measured.

In the third step, RVAD support was applied both in series and parallel mode with rotational speed of 2000, 2500, 3000, 3500, and 4000 rpm. In the fourth step, the slope of the right ESPVR was changed from 0.3 to 0.8 mmHg/mL (0.1 mmHg/mL stepwise increase) during RVAD support connected in series and parallel mode. The measured parameters were those described above.

Considering that we did not measure data in patients undergoing RVAD support to allow us to reproduce their haemodynamic conditions with our numerical simulator, and given that literature data are largely incomplete, we decided against a direct data comparison. Therefore, we considered percentage variation to evaluate the trend of the effects induced by RVAD support on the haemodynamic and energetic variables in line with other available simulation work.

3. Results

Figure 2 shows the effects induced by different values for ESPVR slope ($E_{es\text{RIGHT}}$) on left and right atrial pressure–volume loop area (left upper panel). The percentage changes calculated with respect to the reference value for $E_{es\text{RIGHT}} = 0.3$ mmHg/mL have been listed. The red bars show the percentage change with respect to the reference value for $PVLA_{L-A}$ increase at high $E_{es\text{RIGHT}}$ values. On the contrary, the $PVLA_{R-A}$ (yellow bars) decreases when the percentage change is referred to high $E_{es\text{RIGHT}}$ values. These results show that when $E_{es\text{RIGHT}}$ increases from 0.3 to 0.8 mmHg/mL, the area of the pressure–volume loop of the right atrium decreases, whilst the area of the pressure–volume loop of the left atrium increases (Figure 3). The left and right lower panel shows the left and right atrial pressure–volume loop obtained with different $E_{es\text{RIGHT}}$ values. The black pressure–volume loop was obtained by setting $E_{es\text{RIGHT}} = 0.3$ mmHg/mL, while the blue pressure–volume loop was obtained by setting $E_{es\text{RIGHT}} = 0.6$ mmHg/mL. The left (left side) and the right (right side) ventricular pressure–volume loops are placed in the upper panels. When $E_{es\text{RIGHT}}$ increases, EW_{L-V} and PVA_{L-V} (left upper panel) increase leading to right-sided shift with increased left ESV and EDV. The effect induced by different $E_{es\text{RIGHT}}$ values on left and right ventricular EW (EW_{L-V} and EW_{R-V}) are reported in Figure 2 (left lower panel). The effect induced on EDV and ESV of the left (right) atrium is reported in the upper (lower) right panel (Figure 2). The effect induced on the right atrial ESV is more evident than the one produced on right atrial EDV. Figure 3 (right upper panel) shows that an increase in $E_{es\text{RIGHT}}$ leads to an increase in right ventricular external work and PVA_{R-V} with left-sided shift and a decrease of both right ESV and EDV. Figure 4 shows the effect induced by RVAD support driven in parallel connection (left panels) on left ventricular PVA_{L-V} (left upper panel) and EW_{L-V} (left lower panel). The effect induced on PVA_{L-V} and EW_{L-V} when the RVAD is driven in series is available in the right panels. The data were measured for different values of $E_{es\text{RIGHT}}$ (0.3, 0.5, and 0.8 mmHg/mL) and with increasing RVAD rotational speed (2000, 2500, 3000, 3500, and 4000 rpm). For each rotational speed and $E_{es\text{RIGHT}}$ values, the percentage changes calculated with respect to the reference value measured in pathological conditions have been listed (Figure 4). The highest percentage changes in PVA_{L-V} and EW_{L-V} (50% or more for both variables) were recorded in a diseased condition with right ventricular elastance set to $E_{es\text{RIGHT}} = 0.3$ mmHg/mL during in-parallel RVAD assistance with pump rotational speed at 4000 rpm. Figure 5 shows the effect induced by in-parallel RVAD support on left ventricular ESV_{L-V} (left upper panel) and EDV_{L-V} (left lower panel). The effect induced on ESV_{L-V} (right upper panel) and EDV_{L-V} (right lower panel) by in-series RVAD support is also available for comparison purposes. When the rotational speed of the pump was set to 2000 rpm, the percentage changes for each value of right ventricular ESPVR slope were no more than 3%. The effects induced by a different rotational speed of the RVAD on left and right atrial pressure–volume loop area are available in Figure 6 for three different values of right ESPVR slope. In addition, for each value of the slope, the effect induced by the pump has been calculated in percentage terms with respect to the value obtained without assistance. In the case of the right atrium, we observed a higher percentage reduction of the loop area (from 2 to 9%) during in-series assistance (left lower panel). In the case of parallel connection (left upper panel), the percentage reduction of the pressure–volume loop area of the right atrium becomes more evident at high values for both the slope and the pump rotational speed. Right heart assistance produces significant effects on the left atrium loop area (right panels). Percentage variations between 20 and 50% are observed when the RVAD is connected in parallel to the right ventricle (right upper panel). Whether in-series or in-parallel assistance is considered, the most significant percentage variations are observed when the right ventricular ESPVR slope is set to $E_{es\text{RIGHT}} = 0.3$ mmHg/mL.

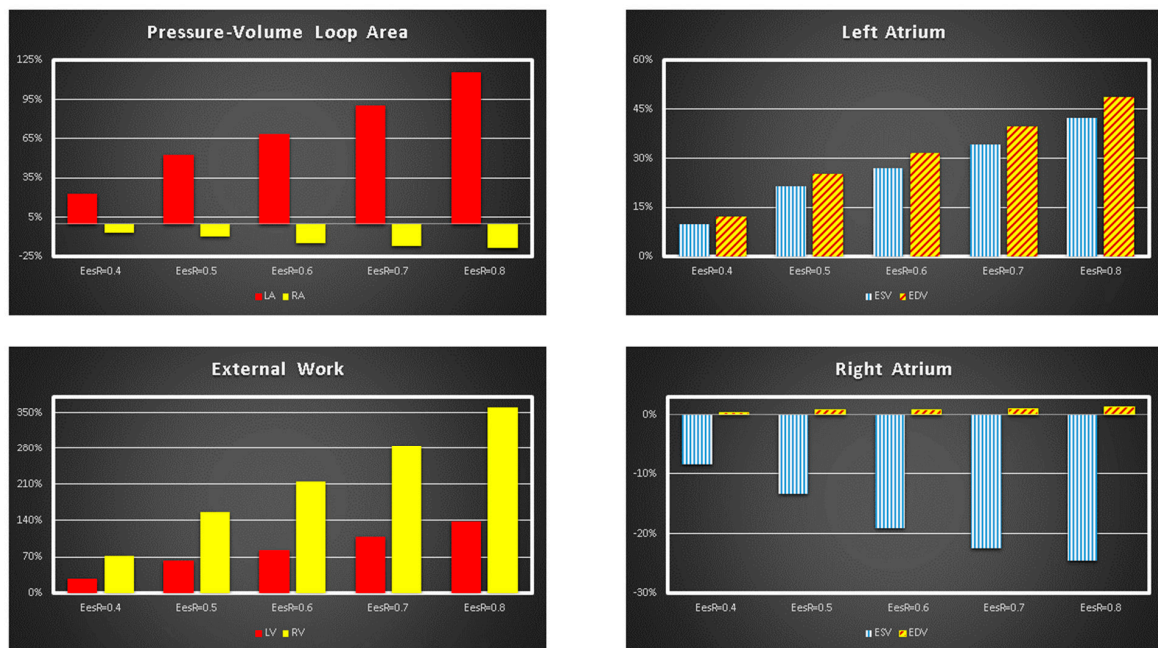


Figure 2. Relative changes calculated in comparison to $Ees_{RIGHT} = 0.3$ mmHg/mL for different Ees_{RIGHT} values (0.4–0.8 mmHg/mL). The relative changes of the pressure–volume loop area of the left and right atrium (external work of the left and right ventricle) are reported in the left upper (lower) panel. The right upper (lower) panel shows the relative changes of left (right) atrial end systolic and end diastolic volume.

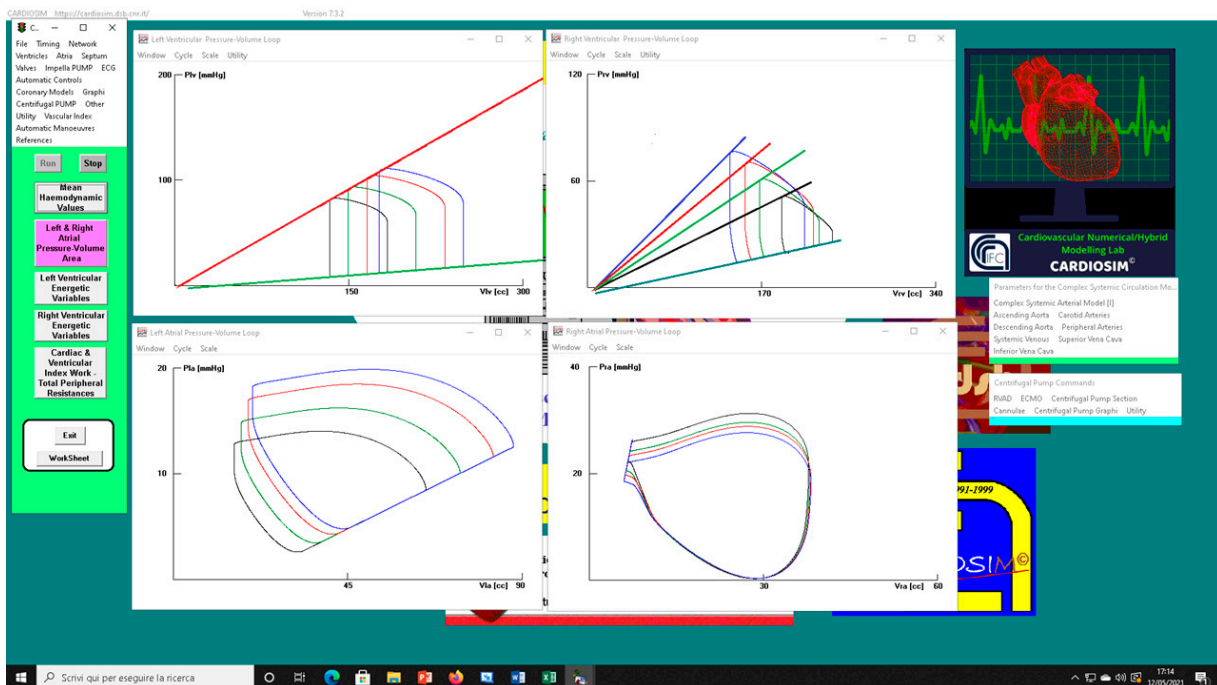


Figure 3. Screen output from CARDIOSIM© software simulator. The left (right) upper panel shows four left (right) ventricular pressure–volume loops obtained by setting $EesR \equiv Ees_{RIGHT} = 0.3$ mmHg/mL (black line), $EesR \equiv Ees_{RIGHT} = 0.4$ mmHg/mL (green line), $EesR \equiv Ees_{RIGHT} = 0.5$ mmHg/mL (red line), and $EesR \equiv Ees_{RIGHT} = 0.6$ mmHg/mL (blue line), respectively. The left (right) lower panel shows four left (right) atrial pressure–volume loops obtained by changing the slope of the right ventricular elastance as previously described.

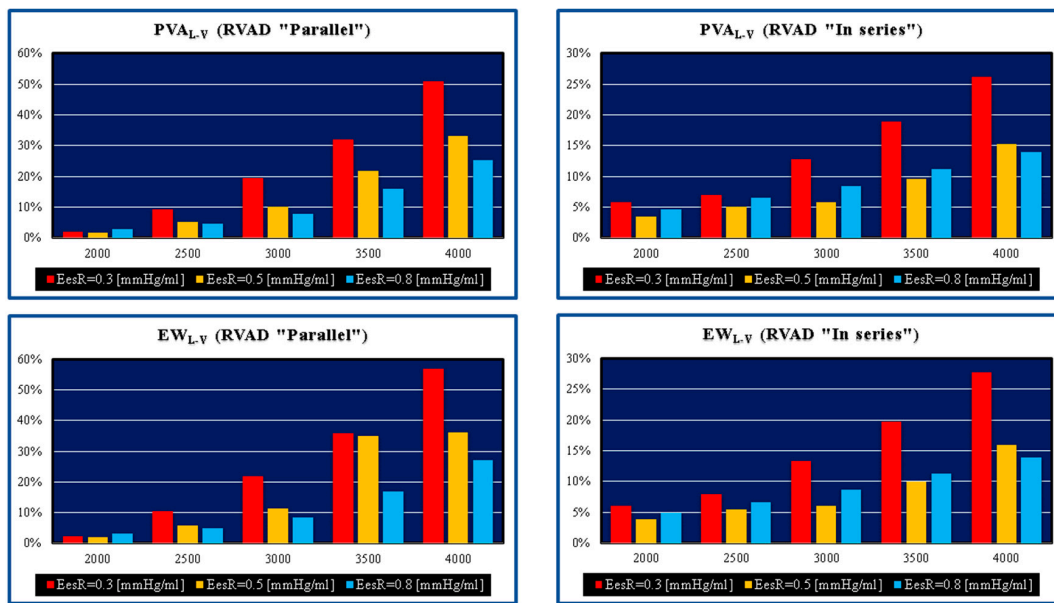


Figure 4. Relative changes calculated in comparison to pathological conditions ($E_{esR} \equiv E_{esR_{RIGHT}} = 0.3, 0.5, \text{ and } 0.8 \text{ mmHg/ml}$) for different types of RVAD connection and different rotational speeds. For each values of $E_{esR_{RIGHT}}$, the relative change was calculated when the RVAD was connected in parallel and in series. The left upper (lower) panel shows the relative changes in the left ventricular pressure–volume area (external work) when the RVAD was connected in parallel to the right ventricle. The right upper (lower) panel shows the relative changes in the left ventricular pressure–volume area (external work) when the RVAD was connected in series to the right ventricle.

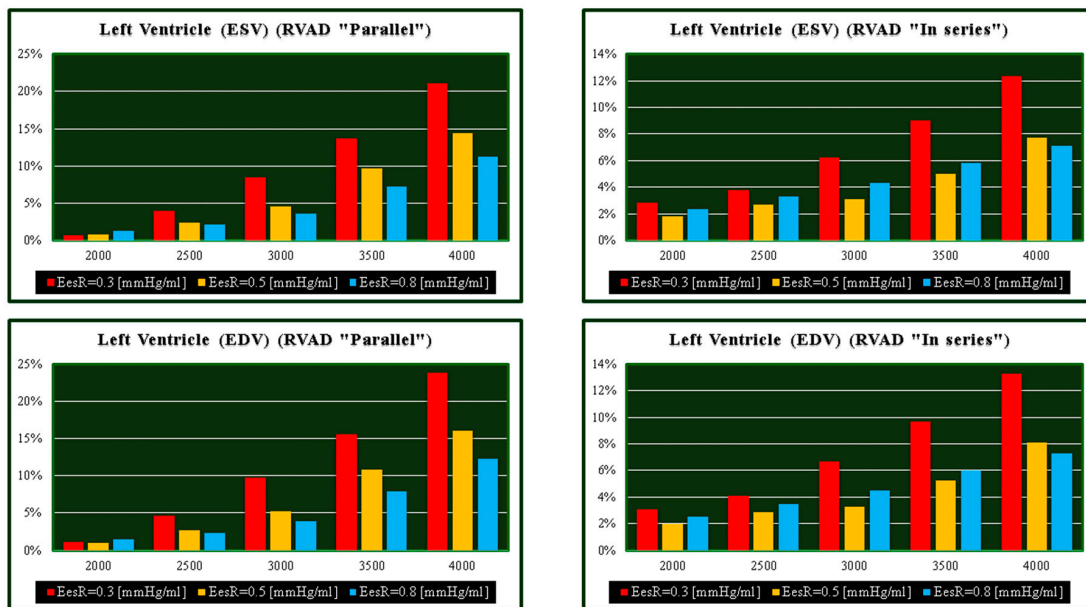


Figure 5. Relative changes calculated in comparison to pathological conditions ($E_{esR} \equiv E_{esR_{RIGHT}} = 0.3, 0.5, \text{ and } 0.8 \text{ mmHg/ml}$) for different types of RVAD connection and different rotational speeds. For each value of $E_{esR_{RIGHT}}$, the relative change was calculated when the RVAD was connected in parallel and “in series” mode. The left upper (lower) panel shows the relative changes in the left ventricular end systolic (end diastolic) volume when the RVAD was connected in parallel to the right ventricle. The right upper (lower) panel shows the relative changes in the left ventricular end systolic (end diastolic) volume when the RVAD was connected in series to the right ventricle.

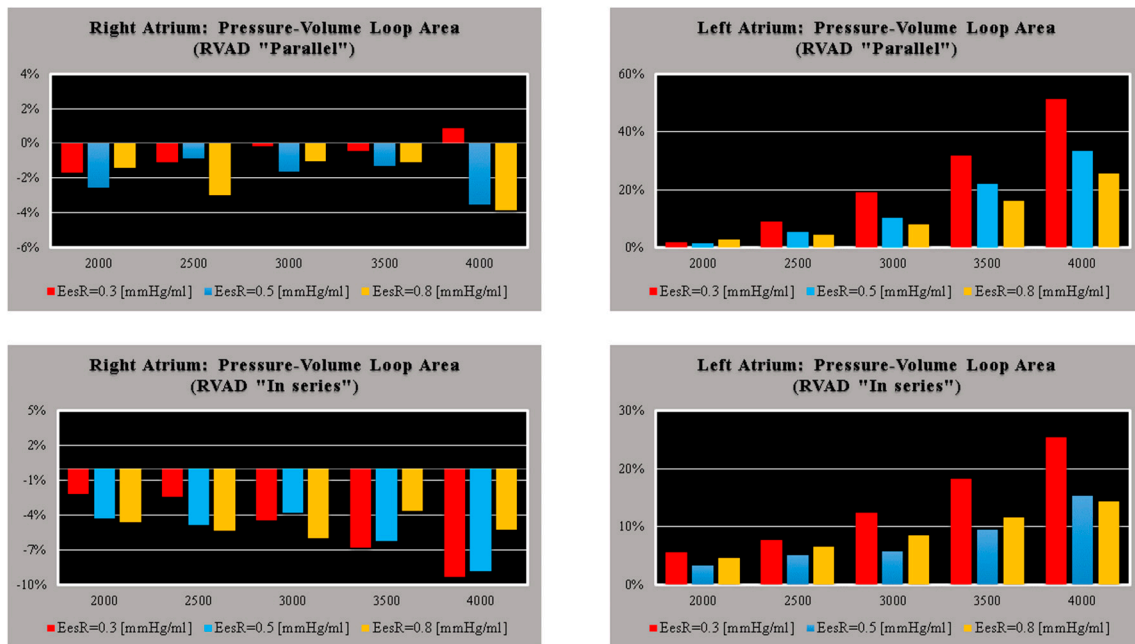


Figure 6. Relative changes calculated in comparison to pathological conditions ($E_{esR} \equiv E_{esR_{RIGHT}} = 0.3, 0.5, \text{ and } 0.8 \text{ mmHg/mL}$) for different types of RVAD connection and different rotational speeds. For each value of $E_{esR_{RIGHT}}$, the relative change was calculated when the RVAD was connected in parallel and in-series mode. The left (right) upper panel shows the relative changes in the right (left) atrium pressure–volume loop area when the RVAD was connected in parallel to the right ventricle. The left (right) lower panel shows the relative changes in the right (left) atrium pressure–volume loop area when the RVAD was connected in series to the right ventricle.

The effects induced by RVAD support on the right ventricular flow output and on the total cardiac output are shown in Figure 7. RVAD parallel assistance generated a lower reduction in right ventricular output compared to in-series assistance for each $E_{esR_{RIGHT}}$ value and each pump’s rotational speed. More specifically, when the pump speed was set to 4000 rpm, parallel assistance induced a reduction between 20 and 45% compared to the baseline value, while the in-series assistance induced a reduction between 38 and 78%. The upper panels in Figure 7 show that parallel RVAD assistance generates a higher increase in total cardiac output compared to in-series assistance at pump speeds higher than 3500 rpm (for each $E_{esR_{RIGHT}}$ value).

The left upper (lower) panel in Figure 8 shows the effects induced on the left ventricular (atrial) loop when different types of RVAD assistance were applied to pathological conditions (black loops) reproduced by setting $E_{esR_{RIGHT}}$ to 0.3 mmHg/mL. The assistance was applied in parallel (red loops) and in series (blue loops) mode with a rotational speed of 3000 rpm.

The right upper (lower) panel shows the effects induced on right ventricular (atrial) loops. When in-parallel assistance was applied, a right-sided shift in the left and right ventricular loop (red lines) was observed. Although in-series RVAD assistance did not cause changes in right end-systolic ventricular volume, it led to a reduction in right end-diastolic ventricular volume. The type of assistance did not cause relevant changes in the right atrial loop (right lower panel).

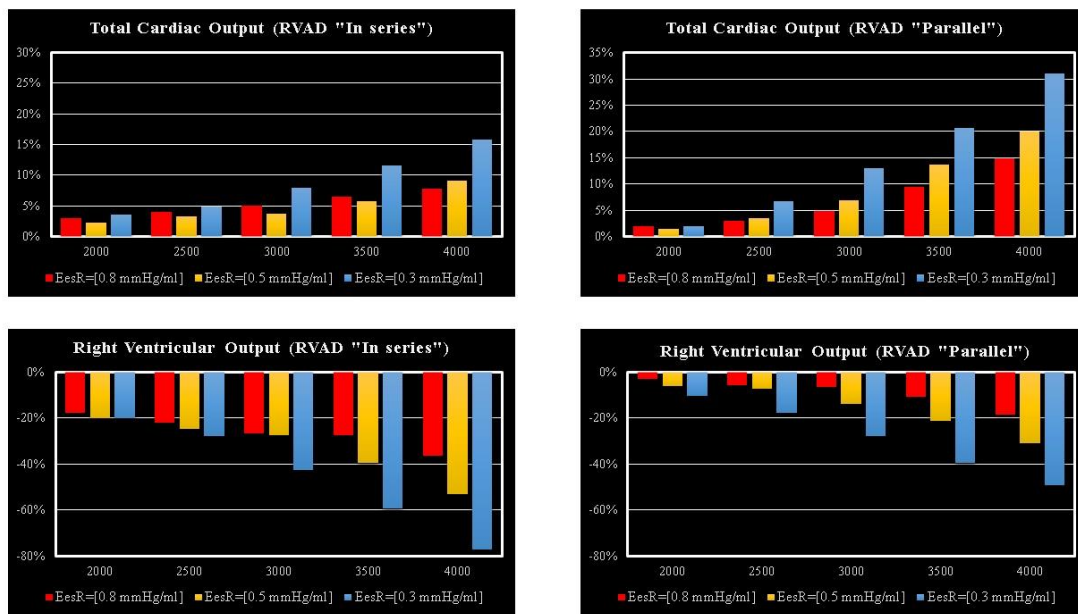


Figure 7. Relative changes calculated in comparison to pathological conditions ($E_{esR} \equiv E_{esR_{RIGHT}} = 0.3, 0.5, \text{ and } 0.8 \text{ mmHg/ml}$) for different types of RVAD connection and different rotational speeds. For each value of $E_{esR_{RIGHT}}$, the relative change was calculated when the RVAD was connected in parallel and in-series mode. The left (right) upper panel shows the relative changes in the total cardiac output (right ventricular flow output plus RVAD flow output) when the RVAD was connected in series (parallel) to the right ventricle. The left (right) lower panel shows the relative changes in the right ventricular flow output when the RVAD was connected in series (parallel) to the right ventricle.

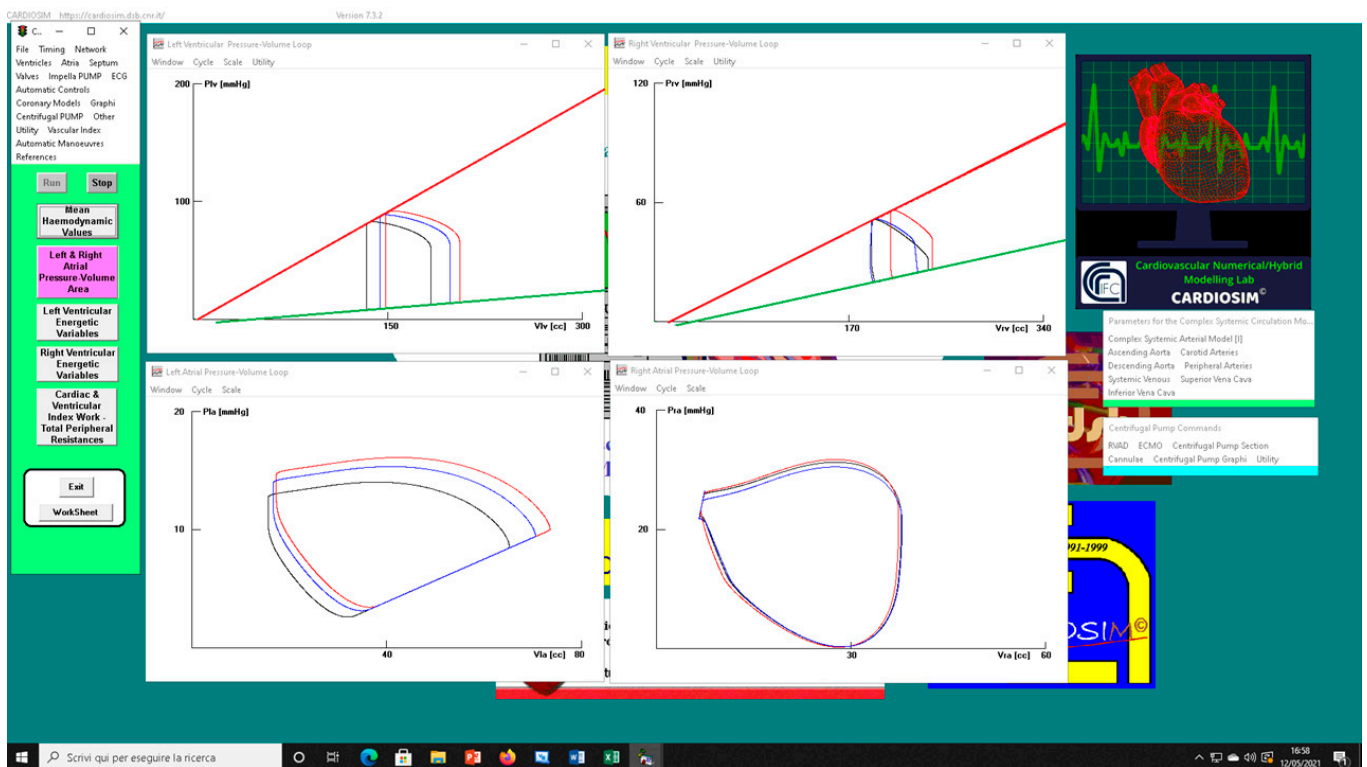


Figure 8. Screen output generated by CARDIOSIM© platform. The left (right) upper panel shows

the left (right) ventricular pressure–volume loops when pathological conditions ($E_{es\text{RIGHT}} = 0.3$ mmHg/mL) (black line), in-parallel RVAD (pump rotational speed at 3000 rpm) (red line), and in-series RVAD assistance (pump rotational speed at 3000 rpm) (blue line) were reproduced by the simulator, respectively. The left (right) lower panel shows the left (right) atrial pressure–volume loops reproduced by CARDIOSIM®.

4. Discussion

The left ventricle (LV) was coupled to the low-compliance, high-resistance peripheral arterial circulation and was more adaptable to changes in pressure than volume. In contrast, the right ventricle (RV) was coupled to the high-compliance, low-resistance pulmonary circulation and was more adaptable to changes in volume than pressure. The right ventricle consisted of a free wall containing a wrap-around circumferential muscle at its base and a septum made of oblique helical fibres crossing each other at 60° angles. This was consistent with the helical ventricular myocardial band concept, which defines two interconnected muscle bands: a basal loop with transverse fibres surrounding the left and right ventricles and an apical loop made of a right- and left-handed helix forming an apical vortex [29,30]. The wrap-around transverse fibres constricted or compressed it from leading to a bellows motion responsible for 20% of right ventricular output, whilst the oblique fibres were responsible for shortening and lengthening, which contributed to 80% of right ventricular systolic function [31]. The crista supra-ventricularis shared muscle fibres with the inter-ventricular septum and the free wall played a key anatomical and functional role [32]. A reduction in longitudinal contraction and an increase in transverse shortening were observed following cardiopulmonary bypass and pericardiotomy [33]. This was quite an important aspect to bear in mind and may be addressed initially with pulmonary vasodilators [34]. The relationship between structure and function plays a key role in clinical decision-making, which must be based on detailed knowledge of normality and recognise how a disease can be addressed to restore normality [31]. The important contribution of right ventricular function has been neglected for a long time due to previous observations and assumptions. The onset of right ventricular dysfunction should trigger the search for the main underlying cause in relation to pressure overload, volume overload, or primary myocardial disease [35]. Right heart failure (RHF) is difficult to manage because of its complex geometry and a lack of specific treatments aimed at stabilisation and recovery of right ventricular function. Nevertheless, right ventricular dysfunction remains associated with poor clinical outcome regardless of the underlying disease mechanism [36].

A simulation approach overcomes ethical issues and the risk of offering an ineffective or potentially dangerous therapeutic option. At the same time, it may help focus on the specific problem to address. Our starting point was to develop a failing right heart, which would require support at a subsequent stage. The easier way to do it was to act on the ESPVR slope of both ventricles. A range between 0.35 and 0.74 mmHg/mL was observed in patients with pulmonary hypertension [10] with a cut-off of 0.8 for E_{es}/E_a ratio as the onset of right ventricular maladaptation. Our initial aim was to observe the effects of RVAD support with either in-series or parallel connection following stepwise variation of right ventricular end-systolic elastance in patients with increased right ventricular afterload. Therefore, the right ventricular end-systolic elastance considered in the present study ranged between 0.3 and 0.8 mmHg/mL as per previously reported values observed in clinical practice [10,37,38]. According to [28], increased native cardiac output was observed in the presence of left ventricular systolic impairment when right ventricular end-systolic elastance increased from 0.1 to 1.0 mmHg/mL. An increased native cardiac output was still observed during VA ECMO support following a stepwise increase in right ventricular end-systolic elastance, but to a lesser degree. A left-to-right ventricular septal shift was observed during diastole following a stepwise increase in right ventricular end-systolic elastance both with and without VA ECMO support. Our considerations were based on the context of pure RVAD support with either in series or parallel connection.

PVA and EW of the left ventricle gain benefit when the pump speed of the RVAD is at least 3500 rpm. The highest effect is obtained when E_{ESRIGHT} is 0.3 mmHg/mL, which is consistent with significant RV dysfunction (left panels in Figure 4). The pathological range considered would suggest that early recognition and aggressive RVAD support is advisable where a lower degree of assistance is required generating enough benefit for a less compromised right ventricle with more potential for recovery. This is an important point to consider in the context of LVAD support when the right heart shows signs of failure requiring attention.

The highest beneficial effect was obtained when the RVAD was connected in parallel to the right ventricle, with up to a nearly 35% increase in total cardiac output (right upper panel in Figure 7) and a lower reduction of right ventricular output compared to in-series RVAD connection. No significant effects were observed on the right atrium regardless of the type of RVAD connection to the right ventricle. Instead, in-parallel RVAD connection had a more beneficial effect on the left atrium. Again, RVAD support has a more beneficial effect on ESV and EDV of the left ventricle when connected in parallel to the right ventricle (left panels in Figure 5). The role of the inter-ventricular septum is critical in this context.

Our aim was to observe the effect of pure RVAD assistance at different stages of right ventricular dysfunction to determine the appropriate timing for intervention. Our target was early graft failure secondary to right heart dysfunction following orthotopic heart transplant and right ventricular failure following LVAD insertion in an apparently preserved right heart function preoperatively. We have focused our attention mainly on E_{ESRIGHT} neglecting V_0 . We have not considered the progressive increase in afterload. Despite this limitation, our preliminary findings support the concept of early intervention in the presence of a failing right heart regardless of its aetiology. This simulation study confirms what had been previously advocated, but not always put into practice [39]. A more liberal right ventricular support may be the way forward [40] when considering different support strategies for a failing right ventricle [41]. Late onset of right ventricular failure remains associated with worse survival and higher cumulative incidence of major adverse events [42].

5. Conclusions

Despite the limitations of a simulation setting and the limited and not homogeneous availability of haemodynamic data measured in patients during RVAD support, this work allowed a trend analysis of haemodynamic and energetic parameters during pure RVAD support with different connection and at different stages of right ventricular dysfunction. Although RVAD support may be effective in advanced right heart failure, early recognition and aggressive treatment is desirable to achieve a more favourable outcome. RVAD support remains an option for advanced right ventricular failure, although the onset of major adverse events may preclude its use. Our simulation work showed that in-parallel RVAD connection to the right ventricle seems a more suitable option.

Author Contributions: Conceptualization, C.D.L. and B.D.L.; Methodology, B.D.L.; Software, C.D.L.; Validation, C.D.L., B.D.L. and M.C.; Formal analysis, B.D.L.; Investigation, C.D.L.; Resources, C.D.L. and M.C.; Data curation, B.D.L.; Writing—original draft preparation, C.D.L.; Writing—review and editing, M.C., C.D.L., A.I., S.P., R.B. and D.F.; Visualization, B.D.L.; Supervision, C.D.L. and M.C.; Project administration, C.D.L.; Analysis of clinical and literature data, A.I., S.P., R.B. and D.F. All authors have read and agreed to the published version of the manuscript.

Funding: This research received no external funding.

Institutional Review Board Statement: Not applicable.

Informed Consent Statement: Not applicable.

Data Availability Statement: Not applicable.

Acknowledgments: Not applicable.

Conflicts of Interest: The authors declare no conflict of interest.

References

- Mandawat, A.; Rao, S.V. Percutaneous Mechanical Circulatory Support Devices in Cardiogenic Shock. *Circ. Cardiovasc. Interv.* **2017**, *10*, e004337. [CrossRef] [PubMed]
- Vullaganti, S.; Tibrewala, A.; Rich, J.D.; Pham, D.T.; Rich, S. The use of a durable right ventricular assist device for isolated right ventricular failure due to combined pre- and postcapillary pulmonary hypertension. *Pulm. Circ.* **2019**, *9*, 1–3. [CrossRef] [PubMed]
- Kaul, T.K.; Fields, B.L. Postoperative acute refractory right ventricular failure: Incidence, pathogenesis, management and prognosis. *Cardiovasc. Surg.* **2000**, *8*, 1–9. [CrossRef]
- Matthews, J.C.; Koelling, T.M.; Pagani, F.D.; Aaronson, K.D. The right ventricular failure risk score a pre-operative tool for assessing the risk of right ventricular failure in left ventricular assist device candidates. *J. Am. Coll. Cardiol.* **2008**, *51*, 2163–2172. [CrossRef] [PubMed]
- Frankfurter, C.; Molinero, M.; Vishram-Nielsen, J.K.K.; Foroutan, F.; Mak, S.; Rao, V.; Billia, F.; Orchanian-Cheff, A.; Alba, A.C. Predicting the Risk of Right Ventricular Failure in Patients Undergoing Left Ventricular Assist Device Implantation. A Systematic Review. *Circ. Heart Fail.* **2020**, *13*, e006994. [CrossRef]
- SAGE Journals. Available online: <https://doi.org/10.1177/02676591211024817> (accessed on 6 April 2022).
- Kiernan, M.S.; Grandin, E.W.; Brinkley, M., Jr.; Kapur, N.K.; Pham, D.T.; Ruthazer, R.; Rame, J.E.; Atluri, P.; Birati, E.Y.; Oliveira, G.H.; et al. Early Right Ventricular Assist Device Use in Patients Undergoing Continuous-Flow Left Ventricular Assist Device Implantation. Incidence and Risk Factors from the Interagency Registry for Mechanically Assisted Circulatory Support. *Circ. Heart Fail.* **2017**, *10*, e003863. [CrossRef]
- Arrigo, M.; Huber, L.C.; Winnik, S.; Mikulicic, F.; Guidetti, F.; Frank, M.; Flammer, A.J.; Ruschitzka, F. Right Ventricular Failure: Pathophysiology, Diagnosis and Treatment. *Card. Fail. Rev.* **2019**, *5*, 140–146. [CrossRef]
- Naeije, R.; Brimiouille, S.; Dewachter, L. Biomechanics of the right ventricle in health and disease (2013 Grover Conference series). *Pulm. Circ.* **2014**, *4*, 395–406. [CrossRef]
- Tello, K.; Dalmer, A.; Axmann, J.; Vanderpoo, R.; Ghofrani, H.A.; Naeije, R.; Roller, F.; Seeger, W.; Sommer, N.; Wilhelm, J.; et al. Reserve of Right Ventricular—Arterial Coupling in the Setting of Chronic Overload. *Circ. Heart Fail.* **2019**, *12*, e005512. [CrossRef]
- Stevenson, L.W.; Hoffman, J.R.H.; Menachem, J.N. The Other Ventricle with Left Ventricular Assist Devices. *J. Am. Coll. Cardiol.* **2021**, *78*, 2309–2311. [CrossRef]
- De Lazzari, C.; Stalteri, D. 2011–2019, CARDIOSIM© Website. Original Website Platform Regarding the Implementation of the Cardiovascular Software Simulator CARDIOSIM©. Available online: <https://cardiosim.dsb.cnr.it/> (accessed on 6 April 2022).
- De Lazzari, C.; Genuini, I.; Pisanelli, D.M.; D’Ambrosi, A.; Fedele, F. Interactive simulator for e-Learning environments: A teaching software for health care professionals. *BioMed Eng. OnLine* **2014**, *13*, 172. [CrossRef] [PubMed]
- De Lazzari, C.; Marconi, S.; Capoccia, M. Physiology of ventricular interdependence. In *Concepts, Mathematical Modelling and Applications in Heart Failure*, 1st ed.; Capoccia, M., De Lazzari, C., Eds.; Nova Science Publisher: New York, NY, USA, 2019; pp. 77–118.
- Capoccia, M.; Marconi, S.; Singh, S.A.; Pisanelli, D.M.; De Lazzari, C. Simulation as a preoperative planning approach in advanced heart failure patients. A retrospective clinical analysis. *BioMed Eng. OnLine* **2018**, *17*, 52. [CrossRef] [PubMed]
- De Lazzari, B.; Iacovoni, A.; Mottaghy, K.; Capoccia, M.; Badagliacca, R.; Vizza, C.D.; De Lazzari, C. ECMO Assistance During Mechanical Ventilation: Effects Induced on Energetic and Haemodynamic Variables. *Comput. Methods Programs. Biomed.* **2021**, *202*, 106003. [CrossRef] [PubMed]
- De Lazzari, C.; De Lazzari, B.; Iacovoni, A.; Marconi, S.; Papa, S.; Capoccia, M.; Badagliacca, R.; Vizza, C.D. Intra-Aortic Balloon Counterpulsation Timing: A New Numerical Model for Programming and Training in the Clinical Environment. *Comput. Methods Programs Biomed.* **2020**, *194*, 105537. [CrossRef]
- Marconi, S.; Capoccia, M.; De Lazzari, C. Mathematical Modelling of the Cardiovascular System. In *Concepts, Mathematical Modelling and Applications in Heart Failure*, 1st ed.; Capoccia, M., De Lazzari, C., Eds.; Nova Science Publisher: New York, NY, USA, 2019; pp. 119–158.
- De Lazzari, C. Interaction between the septum and the left (right) ventricular free wall in order to evaluate the effects on coronary blood flow: Numerical simulation. *Comput. Methods Biomech. Biomed. Eng.* **2012**, *15*, 1359–1368. [CrossRef]
- Capoccia, M.; Marconi, S.; De Lazzari, C. Decision-making in advanced heart failure patients requiring LVAD insertion: Can preoperative simulation become the way forward? A case study. *J. Biomed. Eng. Inform.* **2018**, *4*, 8–20. [CrossRef]
- De Lazzari, C.; Stalteri, D. 2011–2019, CARDIOSIM© Website. Available online: <https://cardiosim.dsb.cnr.it/CirculationModels/pci4> (accessed on 6 April 2022).
- De Lazzari, C.; Stalteri, D. 2011–2019, CARDIOSIM© Website. Available online: <https://cardiosim.dsb.cnr.it/CirculationModels/ncm2> (accessed on 6 April 2022).
- Ottesen, J.T.; Danielsen, M. *Mathematical Modelling in Medicine*, 1st ed.; IOS Press: Amsterdam, The Netherlands, 2000; pp. 1–235.
- Dell’Italia, L.J.; Walsh, R.A. Application of a time varying elastance model to right ventricular performance in man. *Cardiovasc. Res.* **1988**, *22*, 864–874. [CrossRef]

25. Brimiouille, S.; Wauthy, P.; Ewalenko, P.; Rondelet, B.; Vermeulen, F.; Kerbaul, F.; Naeije, R.R. Single-beat estimation of right ventricular end-systolic pressure-volume relationship. *Am. J. Physiol. Heart Circ. Physiol.* **2003**, *284*, H1625–H1630. [[CrossRef](#)]
26. Starling, M.R. Left ventricular-arterial coupling relations in the normal human heart. *Am. Heart J.* **1993**, *125*, 1659–1666. [[CrossRef](#)]
27. Kiani, A.; Gilani Shakibi, J. Normal Values of Left Ventricular End-Systolic Elastance in Infants and Children. *Iran J. Med. Sci.* **2003**, *28*, 169–172.
28. Donker, D.W.; Sallismani, M.; Bromé, M. Right–Left Ventricular Interaction in Left-Sided Heart Failure with and Without Venous Extracorporeal Membrane Oxygenation Support—A Simulation Study. *ASAIO J.* **2021**, *67*, 297–305. [[CrossRef](#)] [[PubMed](#)]
29. Kocica, M.J.; Corno, A.F.; Carreras-Costa, F.; Ballester-Rodes, M.; Moghbel, M.C.; Cueva, C.N.; Lackovis, V.; Kanjuh, V.I.; Torrent-Guasp, F. The helical ventricular myocardial band: Global, three-dimensional, functional architecture of the ventricular myocardium. *Eur. J. Cardiothorac. Surg.* **2006**, *29*, S21–S40. [[CrossRef](#)] [[PubMed](#)]
30. Buckberg, G.; Hoffman, J.I.E.; Mahajan, A.; Saleh, S.; Coghlan, C. Cardiac mechanics revisited: The relationship of cardiac architecture to ventricular function. *Circulation* **2008**, *118*, 2571–2587. [[CrossRef](#)] [[PubMed](#)]
31. Buckberg, G.; Hoffman, J.I.E. Right ventricular architecture responsible for mechanical performance: Unifying the role of ventricular septum. *J. Thorac. Cardiovasc. Surg.* **2014**, *148*, 3166–3171. [[CrossRef](#)]
32. James, T.N. Anatomy of the Crista Supraventricularis: Its Importance for Understanding Right Ventricular Function, Right Ventricular Infarction and Related Conditions. *J. Am. Coll. Cardiol.* **1985**, *6*, 1083–1095. [[CrossRef](#)]
33. Raina, A.; Vaidya, A.; Gertz, Z.M.; Chambers, S.; Forfia, P.R. Marked changes in right ventricular contractile pattern after cardiothoracic surgery: Implications for post-surgical assessment of right ventricular function. *J. Heart Lung Transpl.* **2013**, *32*, 777–783. [[CrossRef](#)]
34. Brown, S.B.; Raina, A.; Katz, D.; Szerlip, M.; Wiegers, S.E.; Forfia, P.R. Longitudinal Shortening Accounts for the Majority of Right Ventricular Contraction and Improves After Pulmonary Vasodilator Therapy in Normal Subjects and Patients with Pulmonary Arterial Hypertension. *Chest* **2011**, *140*, 27–33. [[CrossRef](#)]
35. Sanz, J.; Sánchez-Quintana, D.; Bossone, E.; Bogaard, H.I.; Naeije, R. Anatomy, Function and Dysfunction of the Right Ventricle. *J. Am. Coll. Cardiol.* **2019**, *73*, 1463–1482. [[CrossRef](#)]
36. Konstam, M.A.; Kiernan, M.S.; Bernstein, D.; Bozkurt, B.; Jacob, M.; Kapur, N.K.; Kociol, R.D.; Lewis, E.F.; Mehra, M.R.; Pagani, F.D.; et al. On behalf of the American Heart Association Council on Clinical Cardiology; Council on Cardiovascular Disease in the Young; and Council on Cardiovascular Surgery and Anaesthesia. Evaluation and Management of Right-Sided Heart Failure. A Scientific Statement from the American Heart Association. *Circulation* **2018**, *137*, e578–e622.
37. Haddad, F.; Hunt, S.A.; Rosenthal, D.N.; Murphy, D.J. Right Ventricular Function in Cardiovascular Disease, Part I. Anatomy, Physiology, Aging and Functional Assessment of the Right Ventricle. *Circulation* **2008**, *117*, 1436–1448. [[CrossRef](#)]
38. Kuehne, T.; Yilmaz, S.; Steendijk, P.; Moore, P.; Groenink, M.; Saaed, M.; Weber, O.; Higgins, C.B.; Ewert, P.; Fleck, E.; et al. Magnetic Resonance Imaging Analysis of Right Ventricular Pressure-Volume Loops. In Vivo Validation and Clinical Application in Patients with Pulmonary Hypertension. *Circulation* **2004**, *110*, 2010–2016. [[CrossRef](#)] [[PubMed](#)]
39. Fitzpatrick, J.R.; Frederick, J.R.; Hiesinger, W.; Hsu, V.M.; McCormick, R.C.; Kozin, E.D.; Laporte, C.M.; O'Hara, M.L.; Howell, E.; Dougherty, D.; et al. Early planned institution of biventricular mechanical circulatory support results in improved outcomes compared with delayed conversion of a left ventricular assist device to a biventricular assist device. *J. Thorac. Cardiovasc. Surg.* **2009**, *137*, 971–977. [[CrossRef](#)] [[PubMed](#)]
40. Fischer, Q.; Kirsch, M. Liberal Right Ventricular Assist Device Extracorporeal Membrane Oxygenation Support for Right Ventricular Failure after Implantable Left Ventricular Assist Device Placement. *ASAIO J.* **2018**, *64*, 741–747. [[CrossRef](#)] [[PubMed](#)]
41. Beller, J.P.; Mehaffey, J.H.; Wegermann, Z.K.; Grau-Sepulveda, M.; O'Brien, S.M.; Brennan, J.M.; Thourani, V.; Badhwar, V.; Pagani, F.D.; Ailawadi, G.; et al. Strategies for Mechanical Right Ventricular Support during Left Ventricular Assist Device Implant. *Ann. Thorac. Surg.* **2021**, *in press*. [[CrossRef](#)]
42. Rame, J.E.; Pagani, F.D.; Kiernan, M.S.; Oliveira, G.H.; Birati, E.Y.; Atluri, P.; Gaffey, A.; Grandin, E.W.; Myers, S.L.; Collum, C.; et al. Evolution of Late Right Heart Failure with Left Ventricular Assist Devices and Association with Outcomes. *J. Am. Coll. Cardiol.* **2021**, *78*, 2294–2308. [[CrossRef](#)]